

Seeing through a Black Box: Toward High-Quality Terahertz Tomographic Imaging via Multi-Scale Spatio-Spectral Image Fusion

Weng-tai Su[†], Ta-Hsuan Chao[†], Shang-Hua Yang[†] and Chia-Wen Lin[†]

[†]Department of Electrical Engineering, National Tsing Hua University, Taiwan

Abstract

Terahertz tomographic imaging has recently arisen significant attention due to its non-invasive, non-destructive, non-ionizing, material-classification, and ultrafast-frame-rate nature for object exploration and inspection. However, its strong water absorption nature and low noise tolerance lead to undesired blurring and distortion of reconstructed terahertz images. Research groups aim to deal with this issue through the use of synthetic data in the training phase, but still, their performances are highly constrained by the diffraction-limited terahertz signals. In this paper, we propose a novel multi-scale spatio-spectral fusion Unet (MS3-Unet) that extracts multi-scale features from the different spectral of terahertz image data for restoration. MS3-Unet utilizes multi-scale branches to extract spatio-spectral features which are then processed by element-wise adaptive filters, and then fused to achieve high-quality terahertz image restoration. Here, we experimentally construct ultra-high-speed terahertz time-domain spectroscopy system covering a broad frequency range from 0.1 THz to 4 THz for building up temporal/spectral/spatial/phase/material terahertz database of hidden 3-D objects. Complementary to a quantitative evaluation, we demonstrate the effectiveness of the proposed MS3-Unet image restoration approach on 3-D terahertz tomographic reconstruction applications.

Table 1. Comparison of features of existing imaging technologies. The ability to see through optically-opaque objects enables tomography. The X-ray would ionize objects, which means not bio-safe. Some methods can identify different materials by its spectroscopy, and it requires the penetration of the object. One imaging method is more favorable if it can be placed on the table (table-top), thereby excluding those methods which requires bulky instruments and placed in a special room such as X-ray and Magnetic Resonance Imaging (MRI).

Method	See through opaque objects	Bio-safe	Material Identification	Table-top system
Camera	×	✓	×	✓
X-ray	✓	×	✓	×
LiDAR	×	✓	×	✓
Ultrasonic	✓	✓	×	✓
MRI	✓	✓	×	×
THz Imaging	✓	✓	✓	✓

becomes one of the most commonly used methods. However, the skin of most objects is optically opaque or semi-opaque, which blocks light to retrieve their interior information and further hinders the development of material technology. Therefore, the need to visualize 3-D formation of things, tomography [20], is gaining popularity among various research and application fields. In this paper, we uncover the 3-D tomography of invisible objects hidden within a container with high reconstruction quality by terahertz (THz) imaging.

Table 1 shows the comparison of different types of high-resolution imaging modalities with a non-contact setting. As camera and Light Detection and Ranging (LiDAR) are widely launched for 2-D/3-D image capturing, due to the intensive scattering and absorption happening nearby object surfaces, these two imaging methods cannot visualize 3-D full profiles of most objects. Research groups have successfully found other electromagnetic spectrum regimes to bring information invisible to visible to address this issue. X-ray imaging is one of the commonly used methods to precisely visualize the interior of objects [3, 5, 1, 4, 24]. Despite its invisible-to-visible capability, high-energy X-ray photons would cause both destructive and ionizing impacts to various material types preventing further investigations with other material characterization modalities. Magnetic

1. Introduction

Ever since the first transistor’s invention, semiconductor-empowered science and technology have revolutionized the way people live. Nowadays, the next wave of material systems - quantum materials, alloys, and biomaterials - have demonstrated their potential to bring another technology leap. It is vital to explore their morphology, composition, physical/chemical properties, and how they interact with other matters or even excitation with a better understanding of new material systems and unlock their full capabilities. Thanks to the advance of visible light sensing (VLS) [23] technology, capturing material information through camera

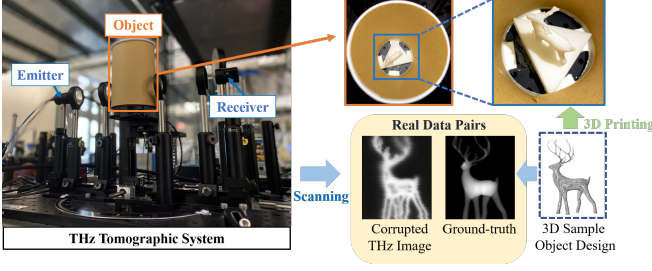


Figure 1. The flowchart THz data collection based on the THz tomographic system.

resonance imaging (MRI) technology is proved as a bio-safe way to visualize soft materials with excellent image contrast. Still, it is bulky and requires sufficient space for operation, which prevents its practical use for most application scenarios. To be pervasively used like visible light cameras, the desired tomographic imaging modality must be operated at a remote distance, non-destructive, bio-safe, compact, and most importantly, capable of digging out information conventional cameras cannot achieve.

THz spectrum, between microwave and infrared, has often been regarded as the last frontier of electromagnetic (EM) wave [29], which provides its unique functionalities among all EM bands. Along with the rapid development of THz technology, THz tomographic imaging has recently arisen significant attention due to its non-invasive, non-destructive, non-ionizing, material-classification, and ultrafast-frame-rate nature for advanced material exploration and engineering. As THz wave can partially penetrate through varieties of optically opaque materials, it carries hidden material tomographic information along the traveling path, making this approach a desirable way to see through black boxes without damaging the exterior [21, 11, 22]. By utilizing intense light-matter-interaction behaviors within the THz band, multifunctional tomographic information of a great variety of materials can also be retrieved even at a remote distance. In the past decades, THz time-domain spectroscopy (THz-TDS) has become one of the most representative THz imaging modalities to achieve non-invasive evaluation because of its unique capability of extracting geometric and multifunctional information of 3-D objects with the size of meter-scale down to atomic-scale. Owing to its fruitful information in multi-dimensional domains - space, time, frequency, phase, and polarization, THz tomography imaging based on THz-TDS has been already allocated for numerous emerging fields, including drug detection [16], industrial inspection, cultural heritage inspection [6] and cancer detection [2].

To retrieve temporal-spatio-spectral information of each object voxel, our THz tomographic imaging experimental setup is based on a THz-TDS system as shown in Fig. 1. Our measured object (a covered 3-D printed deer) is placed on the THz path between THz source and detector of the

THz-TDS system. Based on our developed THz tomographic model, we have successfully reconstructed this hidden deer with high quality tomographic images. The details of our algorithm and its performance would be comprehensively evaluated in the following sections. Fig. 2 shows the raw data directly measured by the THz-TDS system. This figure illustrates time-domain THz signals measured in air, the body, and leg of our 3-D printed deer, respectively. While the THz beam passing through the object, the attenuated THz time-domain signal is encoded with the thickness and material information of the THz-illuminated region. By processing peak amplitudes of THz signals (Time-max), the 3-D profile of the printed deer can be further reconstructed. Although this conventional way is well-fitted for visualizing 3-D objects, the inherent diffraction behavior and strong water absorption nature of THz wave induce various kinds of noise sources as well as the loss of material information. This leads to the undesirable blurring, distorted, speckled phenomenon of functional THz images. Existing works have tackled this issue to restore clear images via estimating point spread functions [25, 26], image enhancement [31], machine learning [18, 32], and more. Their performance is, however, still severely constrained by diffraction-limited THz beam. As a result, the motivation of our work is to reconstruct deep-subwavelength tomographic images by using deep-learning-based image restoration method and spatio-spectral information of the hidden objects.

As shown in Fig. 2, each 2-D THz image is composed by an array of time-domain pulse signals with a temporal resolution of 10 fs. Through Fourier transform operation, we can extract pixel-wise multi-spectral features from the distributed time-domain THz signals. Since the travelling THz beam is significantly attenuated at water absorption frequencies, reconstructed THz images based on water absorption lines offers better details on contoured regimes, resulting in a relatively vivid image contrast. The water absorption frequencies used in this paper are [0.38, 0.448, 0.557, 0.621, 0.916, 0.970, 0.988, 1.097, 1.113, 1.163, 1.208, 1.229] THz as in [30] since higher water absorption frequencies contain too much noise. These spectral (frequency-domain) information of THz images is extracted and then employed to restore clear 2-D images. To more specific, Fig. 3 illustrates multiple 2-D THz images of the same object at different water absorption frequencies, showing very different contrasts and spatial resolutions as these hyperspectral THz image sets have different physical characteristics interacting with objects. The lower-frequency spectral shows higher contrast, whereas the higher-frequency spectral offers better spatial resolution (i.e., from left to right in Fig. 3). Since the low frequency THz signal excels in providing high contrast information, that is, the thickness information of the object, it defines the depth map of the object. In the contrast, the high frequency

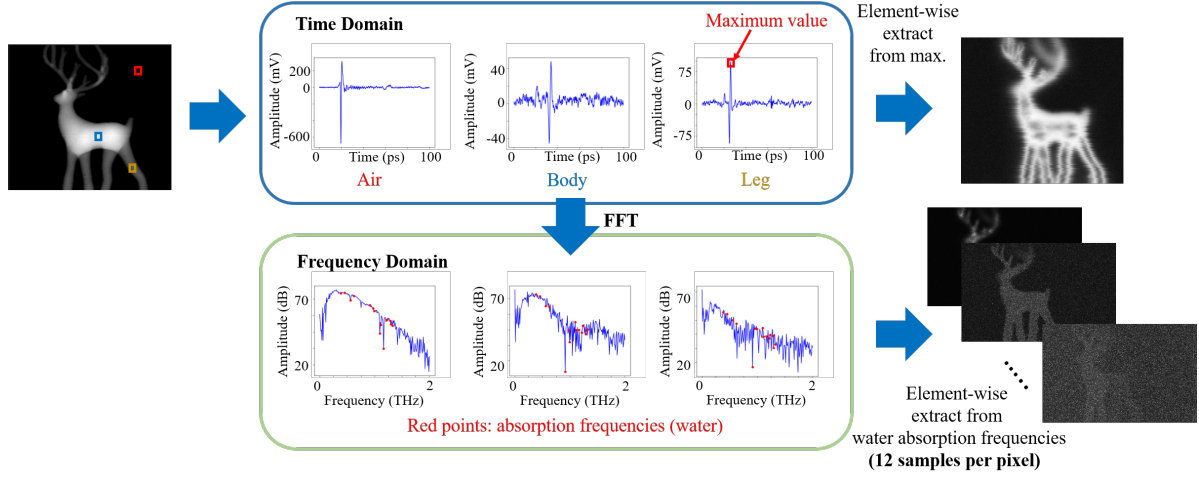


Figure 2. Raw data of measured THz images. This figure illustrates the time domain data measured in air and the body and leg of our 3-D printed deer. The red points illustrate the frequency bands with strong water absorption. The right figures illustrate the reconstructed image using max value of time domain (upper right), and reconstructed image using different water absorption frequencies (lower right).

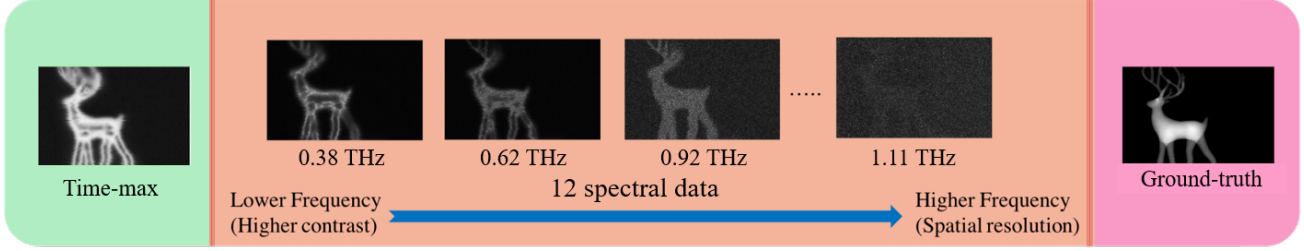


Figure 3. The visualization for multiple images of the same object re-trieved from different frequency spectral of a THz image.

mainly provides more detailed information, that is, the edge and position information of the object, which mean to provide the mask of object location. With these multi-spectral properties of THz images, we can extract rich information from a wide spectral range in the frequency domain to simultaneously restore the 2-D THz images without any additional computational cost or equipment, which is beneficial for further development of THz tomographic imaging.

In this paper, we propose a multi-scale spatio-spectral fusion Unet (MS3-Unet) utilizing the mutual interaction properties of object, EM wave, and environment within THz band. The key idea is to remotely retrieve material information deep inside the objects through light-matter-interaction then distinguish spatial information of each voxel through image restoration. With clear 2-D images restored from corrupted THz images of objects captured from different projections, we can simply achieve high-quality 3-D THz tomography based on restored 2-D images through inverse Radon transform without using any other 3-D reconstruction models.

Our main contributions are summarized as follows:

- An efficient multi-scale spatio-spectral Unet, namely MS3-Unet, is proposed to deal with the image restora-

tion task. By employing multi-spectral features in our network architecture, MS3-Unet significantly outperforms state-of-the-art algorithms in terms of restoration performance.

- Experimentally construct an ultra-high-speed, high signal-to-noise ratio (SNR) THz-TDS system covering a broad frequency range from 0.1 THz to 4 THz. This customized tool is designed to build up temporal/spectral/spatial/phase/material THz database of hidden 3-D objects for further image restoration.
- Provide comprehensively quantitative/qualitative analysis among the proposed MS3-Unet model and state-of-the-art methods. Our MS3-Unet significantly outperforms Time-max, baseline U-Net (Unet-Base), and the multi-spectral U-Net (Unet-MS) by 11.95dB, 2.67dB, and 1.41dB in averaging PSNR.

2. Related Work

In this section, we review works related to our research. First, we review some tomographic image reconstruction for X-ray and computed tomography (CT). Then, we review some deep learning-based restoration.

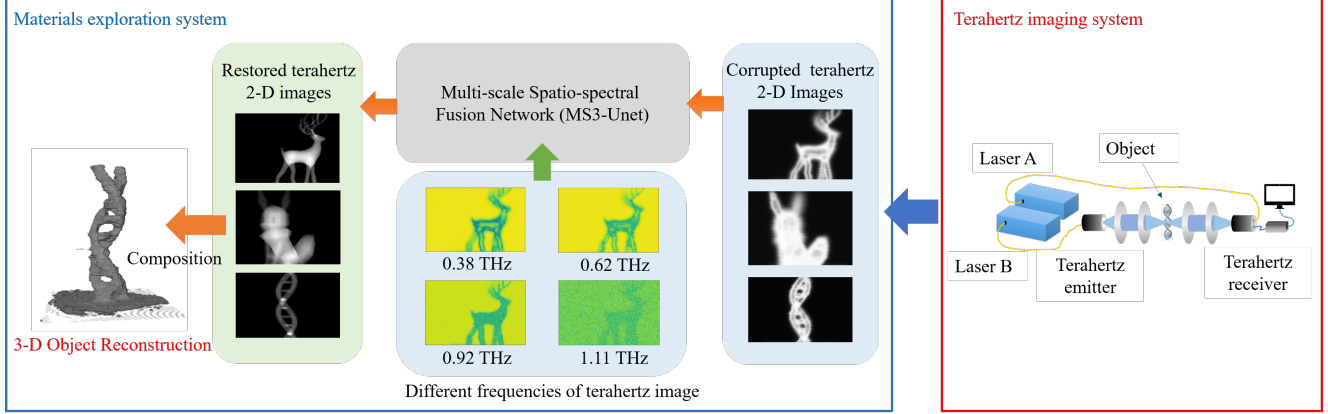


Figure 4. Illustration of a THz tomographic system framework composed of a THz imaging system and material exploration system.

2.1. Tomographic Reconstruction

The method of CT started from X-ray imaging, and many methods of THz imaging are similar to those of X-ray imaging. One of the first works to treat X-ray CT as an image-domain learning problem was [15], and used CNN refine tomographic images. [13] used the U-Net to refine image restoration with great performances. The works above use a scanned layer as an image, and use computer vision techniques to do post-processing. [40] further projects sinograms measured directly from X-ray into higher space and used domain transform to reconstruct images. The aforementioned works have outstanding performance on CT, but they are designed for X-ray imaging. Motivated by those previous works, we incorporated properties of THz waves into deep learning restoration models.

2.2. Deep Learning-based Restoration

In recent years, deep learning methods were first popularized in high-level visual tasks, and then gradually penetrated into many medical tasks such as image restoration, segmentation applications. For example, [34] use the encoder-decoder network architecture to compression the input data into the latent representation, and then the decompression reconstruct the output data into a complete dataset, which had been mainly used to restore full dose CT images from low dose images. In PET/MR applications, [17] employ attenuation correction and MR images to generate synthetic CT images. [33] proposed to use neural network (NN) to estimate the fusion parameters according to the maximum a posteriori (MAP) with different regularization weights for PET restoration, and [12] used the maximum likelihood expectation maximization (MLEM) for dynamic PET imaging, a reconstruction framework based on stacked sparse autoencoders. All of the above work is used the deep learning-based restoration to restore image quality and reduce image artifact such as tomography of X-ray, CT, and PET/MRI.

In additional, the convolutional neural network (CNNs)

has also been proven to achieve the state-of-the-art performance in fundamental image restoration problem [35, 19, 38, 36, 28]. As an extension, several architectures for image restoration are proposed, such as U-Net [28], hierarchical residual network [19] and residual dense network [38]. The proposed DnCNN [35] uses convolution operation, BN, and ReLU to build 17 layers network for image restoration which not only utilized with blind image denoising, but also employed image super-resolution task and JPEG image deblocking. FFDNet [36] used noise level maps as inputs which used a single model to solve multiple noise levels variants. [19] proposed a very deep residual encoding-decoding (RED) architecture which utilized skip connections to solve the image restoration problem via training the very deep network. [38] proposed a residual dense network (RDN), which maximize the reusability of features by using residual learning and dense connection.

As shown in Fig. 2, the image obtained from the THz tomography system is similar to the general image from camera, thus, it can be treated as an image-domain learning problem. To the best of our knowledge, few works use this characteristic to improve image quality of THz imaging. Research works on image-based THz imaging include [25, 26, 31], and tomography works include [9, 8]. In this paper, we use deep learning-based image restoration to solve this problem, especially how to use the rich spectral information of THz images to facilitate the restoration and reconstruction of THz images. Inspired by the U-Net [28] of multi-scale feature extraction, our work extend a similar idea of extracting multi-scale features from the different input frequency spectral data. In order to extract multi-scale spectral features more effectively, we use the Filter Adaptive Convolutional Layer (FAC) [39] to generate different element-wise adaptive filter for each spectral channel. Therefore, these extracted spectral features can easily connect with the different scale branch of U-Net which can fuse the spatio-spectral features to obtain better reconstruction results.

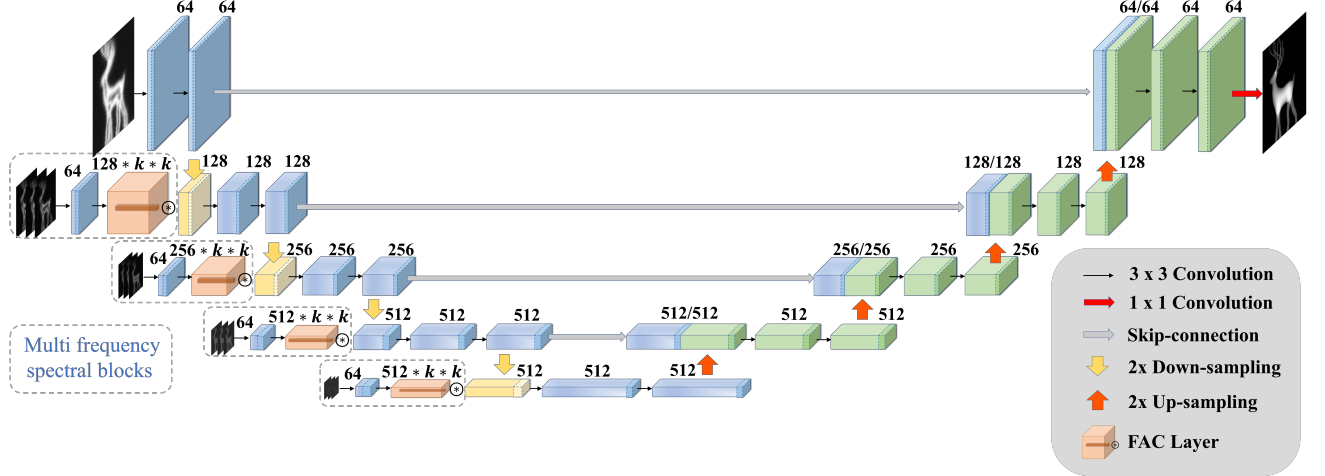


Figure 5. Network architecture of MS3-Unet which includes five scale branches. Except for the first scale using Time-max as input, each scale from second to fifth utilize 3 spectral as input.

3. Terahertz Tomographic Imaging

In this section, we first present the overall framework of our proposed MS3-Unet in Sec. 3.1. Then, we show the network structure of MS3-Unet in Sec. 3.2. In the third part, we present the loss function which are used to train the network in Sec. 3.3. Lastly, we introduce the THz tomography to reconstruct 3-D imaging (tomography) in Sec. 3.4.

3.1. Overview

As illustrated in Fig. 4, our THz tomographic imaging system aims to reconstruct a clear 3-D object from its corrupted THz 2D images. To this end, the pixel-wise spectral information carried in THz-TDS 2D images, when a corrupted THz 2D image does not contain enough reconstruction information, similar to spatio-temporal video deblurring, we can leverage the information of predominant spectral bands to complement the conventional Time-max image, that records the maximum amplitude of the time-domain THz signal of each pixel for restoration. Therefore, we propose a multi-scale spatio-spectral fusion network (MS3-Unet), that utilizes Filter Adaptive Convolutional Layer (FAC) [39] to extract the spectral information and complement the corrupted THz 2D image to achieve better restoration results. Finally, we utilize the Random Transform to reconstruct clear 3-D objects from these restored clear 2-D images.

3.2. Network Architecture

To extract multi-scale spatio-spectral features, as illustrated in Fig. 5, on top of the U-Net, our MS3-Unet consists two parts: i) the encoder that accepts the corrupted THz 2D image (Time-max) as the input of the finest-scale branch and then feeds the additional predominant spectral bands to the second to fifth scale branches of the network

(each scale receives 3 spectral bands in our method). Then, we utilize the Filter Adaptive Convolutional Layer (FAC) in each scale to extract and fuse the multi-scale features from the different input spectral data, as indicated by the gray dotted lines. These filters (i.e., brown color block in Fig. 5) perform element-wise adaptive filtering for each channel which are more effective to extract spectral information. Then, these extracted spectral features, along with the down-sampled features of the upper layer, are fused together. ii) the right-half decoder received the fused multi-scale multi-spectral features and then derives the restored THz 2D images, where the skip connections stitch the shallow features (blue blocks) with the deep features (green blocks).

Note, a finer-scale branch of MS3-Unet extracts shallower-layer features which usually capture the low-level features of an object, such as colors and edge. Therefore we feed into finer-scale branches with the lower spectral-bands which mainly provide high-contrast features, e.g., the thickness of object pixels, carrying the depth information of the object. In contrast, a coarser-scale branch captures deeper-layer semantic-level features of an object. The high spectral-bands which mainly provide contours and position information of an object, can better complement the object’s semantic-level features. Therefore, in MS3-Unet, the encoder extracts multi-scale features from the THz images of 12 selected spectral bands, in addition to the Time-max image. We feed the Time-max signal as the input of the finest-scale branch, then feed the 12 spectral bands to the remaining four branches (three bands to each scale): lower-frequency bands to finer-scale branches.

3.3. Loss Function

To effectively train the proposed MS3-Unet, we employ the following mean squared error (MSE) loss that measures the differences between the \mathbf{X}_{out} and \mathbf{X}_{GT} :

$$\mathbf{L}_{MSE}(\mathbf{X}_{\text{GT}}, \mathbf{X}_{\text{out}}) = \frac{1}{HW} \sum_{i=1}^H \sum_{j=1}^W (\mathbf{X}_{\text{GT}}(i, j) - \mathbf{X}_{\text{out}}(i, j))^2, \quad (1)$$

where \mathbf{X}_{GT} denotes ground-truth image, \mathbf{X}_{out} is the restored image, H is the height and W is the width of the image.

3.4. THz Tomography Reconstruction

The 3D tomography of an object is reconstructed from the THz 2-D images of the object scanned in different angles. To this end, the object is placed on a rotational plate and turn the plate by θ angle from 0° to 360° . In each angle, we scan a $W \times H$ array of THz time-domain pulses, which are usually corrupted and blurred due to physical characteristics of THz waves mentioned previously. We restore each array of THz data using our proposed MS3-Unet to address the problem of undesired blurs and noises in THz images. To convert 2-D images into a 3-D tomographic image, we adopt the well-known inverse Radon transform.

We define the width of the sample on the x -axis, the height on the y -axis, and the depth on the z -axis. The scanning of an image represents the line integral on the z -axis, and forming an image on the $x - y$ plane. Now, we take one slice on the $x - z$ plane for analysis. To reconstruct a 3D tomography, each pixel on the $x - z$ plane is needed, we thus define $f(x, z)$ as one slice on the $x - z$ plane. We define the scanning as line integral along line $L(\theta, t)$, where t moves along the $x - axis$ within the θ angle. As a result, we obtain the following intensity distribution $P(\theta, t)$:

$$P(\theta, t) = \int_{L(\theta, t)} f(x, z) dl, \quad (2)$$

The intensity distribution $P(\theta, t)$ is called the sinogram, and Eq. (2) is called the Radon transform. Since the function of the desired plane is $f(x, z)$, we can directly utilize the inverse Radon transform to obtain the 3-D tomography, using methods like filtered back-projection (FPB) [14] or the simultaneous algebraic reconstruction technique (SART) [27].

4. Experiments

We conduct experiments to evaluate the effectiveness of our MS3-Unet against existing state-of-the-art image restoration methods. We first present our experiment settings and then evaluate the advantages of the proposed multi-scale spatio-spectral feature fusion on THz image restoration.

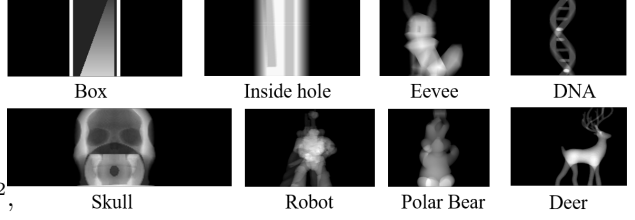


Figure 6. Illustration of authentic measured THz data for the eight 3D-printed HIPS objects in our experiments.

4.1. THz-TDS Image Dataset

As shown in Fig. 1, we prepare our sample objects by a Printech 3-D printer, and use the material of high impact polystyrene (HIPS) for 3D-printed the objects due to its high penetration of THz waves. We then use our in-house Asynchronous Optical Sampling THz time-domain spectroscopy (ASOPS THz-TDS) [10] system to measure the sample objects. Each sample object is placed on a motorized stage between the source and the receiver. With the help of the motorized stage, a raster scan is applied to each object in multiple projection angles. In the scanning phase, we scan the objects with a rotational range of 180 degrees with 6 degrees each step, a horizontal range of 72mm with 0.25mm each step, and a variable vertical range according to the object height with 0.25mm each step. In this way, we obtain 30 projections of each object, which are then augmented to 60 projects by horizontal flipping.

The ground-truth of the data is obtained by converting the original 3-D printing files into image projections in every angle. We use markers to point out the center of rotation so that we can align the ground-truth images with the measured THz data. In this paper, totally eight objects are printed, measured, and aligned for use.

4.2. Data Processing and Augmentation

In our experiments, we train the proposed MS3-Unet using the 2-D THz images from our THz tomographic system shown in Fig. 4. The data contains 8 objects in Fig. 6: 60 projections per object and 480 2D THz images in total. In order to thoroughly evaluate the capacity of network, we use leave-one-out strategy which use the data of 7 objects as the training set, and remaining object as the testing set. Due to the limited space, we only present the results for **Deer** and **DNA** here, and the remaining results in the supplementary material. We will release our code and the THz image dataset.

We also perform typical data augmentations to enrich the training set for THz image restoration, involving random transformations on brightness, contrast, and saturation, image scaling with a scaling factor ranging in $[0.5, 1.5]$, and geometric transformations including random flipping horizontally and vertically. Finally, the images are randomly cropped to 120×120 patches.

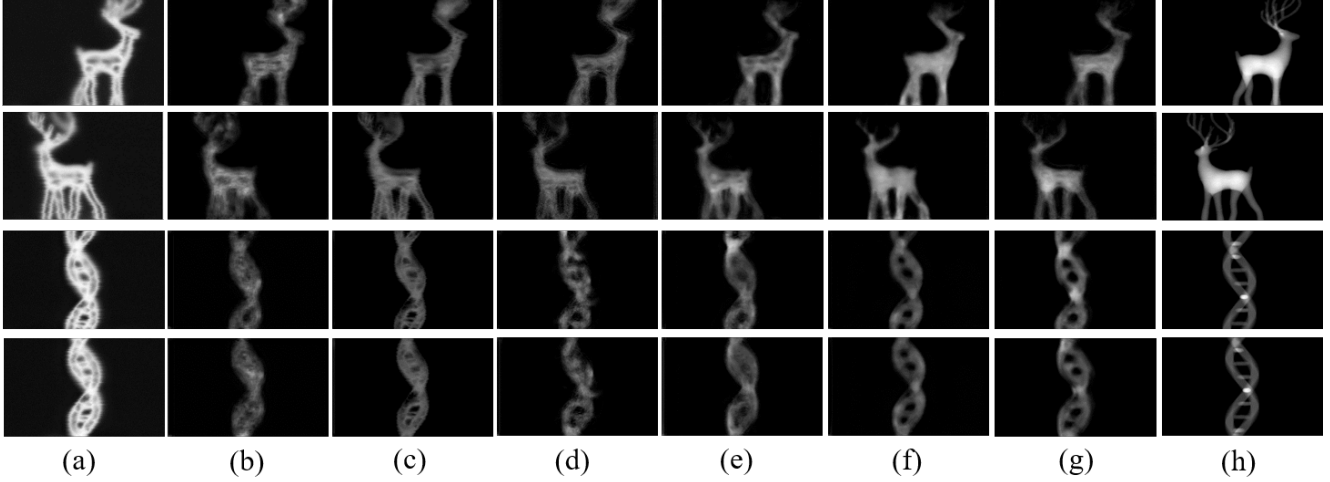


Figure 7. Qualitative comparison of THz image restoration results for **Deer** and **DNA**, from left to right: (a) Time-max, (b) DnCNN-S [35], (c) RED [19], (d) RDN [38], (e) base-Unet [28], (f) MS-Unet, (g) MS3-Unet (ours), and (h) the ground-truth.

Table 2. Quantitative comparison (PSNR, SSIM, and LPIPS) of THz image restoration performances for **Deer** and **DNA** with different restoration methods. \uparrow : higher is better; \downarrow : lower is better

Method	PSNR \uparrow		SSIM \uparrow		LPIPS \downarrow	
	Deer	DNA	Deer	DNA	Deer	DNA
Time-max	12.42	12.07	0.05	0.05	0.36	0.28
DnCNN-S [35]	19.94	23.95	0.73	0.77	0.19	0.16
RED [19]	19.30	24.17	0.81	0.83	0.22	0.14
RDN [38]	19.49	24.44	0.78	0.78	0.17	0.18
base-Unet [28]	19.84	24.15	0.55	0.78	0.17	0.11
MS-Unet	21.37	24.72	0.71	0.80	0.17	0.11
MS3-Unet (Ours)	22.02	26.32	0.83	0.85	0.12	0.10

Table 3. Quantitative comparison (PSNR, SSIM, and LPIPS) of THz image restoration performances for **Deer** and **DNA** with different settings. \uparrow : higher is better; \downarrow : lower is better

Method	PSNR \uparrow		SSIM \uparrow		LPIPS \downarrow	
	Deer	DNA	Deer	DNA	Deer	DNA
base-Unet [28]	19.84	24.15	0.55	0.78	0.77	0.11
MS3-Unet ₄	21.13	25.53	0.82	0.85	0.14	0.11
MS3-Unet _{12rand}	21.83	25.76	0.83	0.82	0.13	0.10
MS3-Unet ₁₂ (Ours)	22.02	26.32	0.83	0.85	0.12	0.10

4.2.1 Experiment Settings

We initialize our MS3-Unet following the initialization method in [7], and train it using Adam optimizer with $\beta_1 = 0.9$ and $\beta_2 = 0.999$. We set the initial learning rate to 10^{-4} and then decay the learning rate by 0.1 every 300 epochs. The proposed network converges after 1,000 epochs. For a fair comparison with the compared algorithms, we adopt their publicly released codes.

4.3. Quantitative Evaluations

To the best of our knowledge, no method is specially designed for restoring THz images besides Time-max. Thus, we compare our method against several widely-used CNN-based image restoration models, including DnCNN [35],

RED [19], and RDN [38]. Moreover, we also compare two variants of U-Net [28]: base-Unet and MS-Unet. base-Unet is the baseline Unet that extract image features in five different scales following the original setting in [28], whereas MS-Unet incorporates multi-spectral features by concatenating the feature of Time-max with additional 12 THz bands as the input (i.e., $12 + 1$ channels) of the finest scale of U-Net. For the objective assessment of THz image restoration, we adopt three widely-used metrics including the Peak Signal-to-Noise Ratio (PSNR), Structural Similarity (SSIM) index, and Learned Perceptual Image Patch Similarity (LPIPS) [37], where the former two respectively measure the pixel-level and structure-level similarities, and the latter measures the perceptual-level distance between a restored image and its ground-truth.

Table 2 shows that the proposed method performs much favorably against the competing methods on two sample objects **Deer** and **DNA** in all the three metrics. Additional results on the remaining sample objects are provided in the supplementary material. Specifically, our MS3-Unet outperforms Time-max, baseline U-Net (base-Unet), and the multi-spectral U-Net (MS-Unet) by 9.60 dB, 3.18 dB, and 0.65 dB in PSNR for **Deer**, and 14.30 dB, 2.17 dB, and 1.60 dB for **DNA**, respectively. For qualitative evaluation, Fig. 7 illustrates two restored views for each of **Deer** and **DNA**, demonstrating that MS3-Unet can restore objects with much finer and smoother details (the antler and legs of **Deer** and the base pairs and shapes of **DNA** double-helix), faithful thickness of material (e.g., the body and legs of **Deer**, the crossings of helices of **DNA**), and fewer artifacts (e.g., holes and broken parts). Both the quantitative and qualitative evaluations confirm a significant performance leap with the proposed multi-scale spatio-spectral feature fusion.

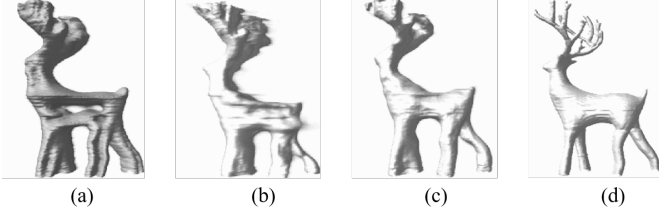


Figure 8. Illustration of 3-D tomographic imaging results for Deer, from left to right: (a) Time-max, (b) baseline U-Net [28], (c) MS3-Unet, and (d) ground-truth.

4.4. Ablation Study

To verify the effectiveness of multi-spectral feature fusion, we evaluate the restoration performances with our MS3-Unet under different settings of spectral bands as listed in Table 3. The compared methods include (1) baseline U-Net (base-Unet) that only utilizes a single channel of data (Time-max) without using features of multi-spectral bands; (2) MS3-Unet_k that concatenates multi-band features in each of the four spatial-scale branches, except for the finest scale (that accepts the Time-max image as the input), where $k = 4, 12$ means that totally 4 (1 band/scale) and 12 additional spectral bands (3 bands/scale) are fed into the four spatial-scale branches with the assignment of the lowest spectral bands to the coarsest scale, and vice versa; and (3) MS3-Unet_{12rand} that takes all the 12 spectral bands, where 3 out of the 12 bands are randomly picked and assigned to each scale branch.

The results clearly show the advantage of multi-spectral feature fusion for THz image restoration. The restoration performance consistently improves when the number of spectral bands k increases (i.e., 1-band Unet-base, 4-band MS3-Unet₄, and 12-band MS3-Unet₁₂), since different-band spectral information can complement each other. Furthermore, the results also show that the order of spectral bands matters — sequentially feeding the spectral bands from low to high frequencies to the fine to coarse scales is better than randomly assigning the spectral-band features.

4.5. 3-D Tomography Reconstruction

The goal of our work is to reconstruct a clear 3-D object through a THz tomographic imaging system by using THz imaging restoration. In our system, the tomography of an object is reconstructed from 30 2-D THz images of an object scanned in different angles, each being restored by MS3-Unet. Then we apply the inverse Radon transform to reconstruct the 3-D THz tomography. Fig. 8 demonstrates the 3-D reconstruction objects of **Deer**. It shows that Time-max and Unet-base cannot well reconstruct sharp details and may lose important details such as the Time-max lost the information in deer’s stomach. In contrast, our results performs the best and restores much clearer 3-D im-

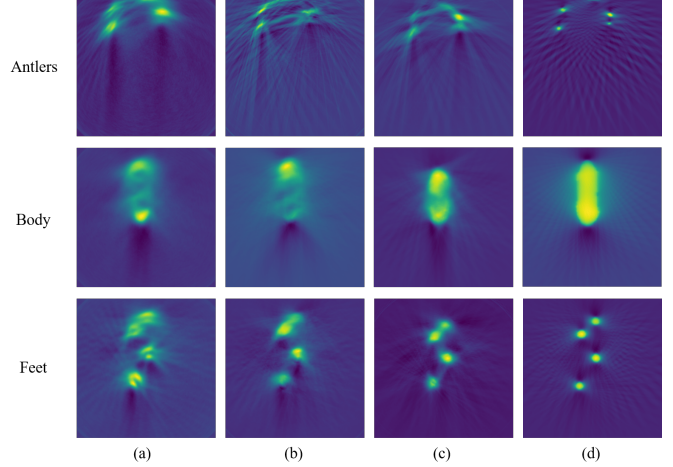


Figure 9. Illustration of 2D slices (antlers, body, and feet) of the 3-D tomography of **Deer** reconstructed by different methods, from left to right: (a) Time-max, (b) Unet-base [28], (c) MS3-Unet, and (d) ground-truth.

ages with more details, achieving by far the best 3-D THz tomography reconstruction quality in the literature. Additional 3-D reconstruction results are provided in the supplementary material.

The reconstructed 3-D object also involves an object’s internal structure. Fig. 9 compares the 2D slices of the reconstructed 3-D tomography of **Deer** reconstructed by three methods for three parts: Antlers, body, and feet, showing that MS3-Unet faithfully retains important internal structures and generates much fewer artifacts compared with the other methods.

5. Conclusion

We proposed a 3-D THz tomographic imaging system based on multi-scale spatio-spectral feature fusion. Based on the physical characteristics of THz waves passing through different materials, our method extracts most predominant spectral features in different spatial scales by seeing through an object. The multi-spectral features are fused by element-wise adaptive filtering for object inspection and exploration in a multi-scale manner. Our experimental results have confirmed a performance leap from the relevant state-of-the-art techniques in the area. We believe our findings in this work will stimulate further applicable research for terahertz tomographic imaging with advanced computer vision techniques.

References

- [1] A. akdinawat and D. Attwood. Nanoscale x-ray imaging. *Nature Photonics*, 4(12):840, 2010. 1
- [2] T. Bowman, T. Chavez, K. Khan, J. Wu, A. Chakraborty, N. Rajaram, K. Bailey, and M. El-Shenawee. Pulsed terahertz

- imaging of breast cancer in freshly excised murine tumors. *J. Biomedical optics*, 23(2):026004, 2018. 2
- [3] D. Chapman, W. Homlinson, R. Johnston, D. Washburn, E. Pisano, N. Gmür, Z. Zhong, R. Menk, F. Arfelli, and D. Sayers. Diffraction enhanced x-ray imaging. *J. Physics in Medicine & Biology*, 42(11):2015, 1997. 1
- [4] P. Cloetens, R. arrett, J. Baruchel, J.-P. Guigay, and M. Schlenker. Phase objects in synchrotron radiation hard x-ray imaging. *J. Physics D: Applied Physics*, 29(1):133, 1996. 1
- [5] R. Fitzgerald. Phase-sensitive x-ray imaging. *Physics Today*, 53(7):23–26, 2000. 1
- [6] K. Fukunaga. *Thz technology applied to cultural heritage in practice*. Springer, 2016. 2
- [7] K. He, X. Zhang, S. Ren, and J. Sun. Delving deep into rectifiers: Surpassing human-level performance on imagenet classification. In *Proc. IEEE/CVF Int. Conf. Comput. Vis.*, pages 1026–1034, 2015. 7
- [8] Y.C. Hung and S.-H. Yang. Kernel size characterization for deep learning terahertz tomography. In *Proc. Int. Infrared. Milli. THz. Wave.*, pages 1–2, 2019. 4
- [9] Y.-C. Hung and S.-H. Yang. Terahertz deep learning computed tomography. In *Proc. Int. Infrad. Milli. THz. Wav.*, pages 1–2. IEEE, 2019. 4
- [10] Christof Janke, Michael Först, Michael Nagel, Heinrich Kurz, and Albrecht Bartels. Asynchronous optical sampling for high-speed characterization of integrated resonant terahertz sensors. *Optics lett.*, 30(11):1405–1407, 2005. 6
- [11] C. Jansen, S. Wietzke, O. Peters, M. Scheller, N. Vieweg, M. Salhi, N. Krumbholz, C. Jördens, T. Hochrein, and M. Koch. Terahertz imaging: applications and perspectives. *Appl. Optics*, 49(19):E48–E57, 2010. 2
- [12] J. Cui, X. Liu, Y. Wang, and H. Liu. Deep reconstruction model for dynamic pet images. *J. PloS One*, 12(9):e0184667, 2017. 4
- [13] K. H. Jin, M. T. McCann, E. Froustey, and M. Unser. Deep convolutional neural network for inverse problems in imaging. *IEEE Trans. Image Process.*, 26(9):4509–4522, 2017. 4
- [14] A. C. Kak. Algorithms for reconstruction with nondiffracting sources. *Principles of computerized tomographic imaging*, pages 49–112, 2001. 6
- [15] E. Kang, J. Min, and J. C. Ye. A deep convolutional neural network using directional wavelets for low-dose x-ray ct reconstruction. *J. Medical physics*, 44(10):e360–e375, 2017. 4
- [16] K. Kawase, Y. Ogawa, Y. Watanabe, and H. Inoue. Non-destructive terahertz imaging of illicit drugs using spectral fingerprints. *Optics Express*, 11(20):2549–2554, 2003. 2
- [17] F. Liu, H. Jang, R. Kijowski, T. Bradshaw, and A.B. McMillan. Deep learning mr imaging-based attenuation correction for pet/mr imaging. *Radiological Society of North America*, 286(2):676–684, 2018. 4
- [18] M. Ljubenovic, S. Bazrafkan, J. De Beenhouwer, and J. Sijbers. Cnn-based deblurring of terahertz images. In *Proce. IEEE Conf. Comput. Vis. Theory Appl.*, pages 323–330, 2020. 2
- [19] X. Mao, C. Shen, and Y.-B. Yang. Image restoration using very deep convolutional encoder-decoder networks with symmetric skip connections. In *Proc. Adv. Neural Inf. Process. Syst.*, page 2802–2810, 2016. 4, 7
- [20] T. M. Buzug. Computed tomography. In *Springer handbook of medical technology*, pages 311–342. Springer, 2011. 1
- [21] D. Mittleman, M. Gupta, R. Neelamani, R. Baraniuk, J. Rudd, and M. Koch. Recent advances in terahertz imaging. *Applied Physics B*, 68(6):1085–1094, 1999. 2
- [22] D. M. Mittleman. Twenty years of terahertz imaging. *Optics Express*, 26(8):9417–9431, 2018. 2
- [23] P. H. Pathak, X. Feng, P. Hu, and P. Mohapatra. Visible light communication, networking, and sensing: A survey, potential and challenges. *IEEE commun. surveys & tutorials*, 17(4):2047–2077, 2015. 1
- [24] J. Peterson, F. Paerels, J. Kaastra, M. Arnaud, T. Reiprich, A. Fabian, R. Mushotzky, J. Jernigan, and I. Sakelliou. X-ray imaging-spectroscopy of abell 1835. *J. Astronomy & Astrophysics*, 365(1):L104–L109, 2001. 1
- [25] D. C. Popescu and A. D. Ellicar. Point spread function estimation for a terahertz imaging system. *EURASIP Journal on Adv. Signal Process.*, 2010(1):575817, 2010. 2, 4
- [26] D. C. Popescu, A. Hellicar, and Y. Li. Phantom-based point spread function estimation for terahertz imaging system. In *Proc. Int. Conf. Adv. Concepts for Intell. Vis. Syst.*, pages 629–639, 2009. 2, 4
- [27] B. Recur, A. Younus, S. Salort, P. Mounaix, B. Chassagne, P. Desbarats, J. Caumes, and E. Abraham. Investigation on reconstruction methods applied to 3d terahertz computed tomography. *Optics express*, 19(6):5105–5117, 2011. 6
- [28] O. Ronneberger, P. Fischer, and T. Brox. U-net: Convolutional networks for biomedical image segmentation. In *Proc. Int. Conf. Medical Image Comput. Computer-Assisted Intervention*, pages 234–241, 2015. 4, 7, 8
- [29] D. Saeedkia. *Handbook of terahertz technology for imaging, sensing and communications*. Elsevier, 2013. 2
- [30] D. M. Slocum, E. J. Slingerland, R. H. Giles, and T. M. Goyette. Atmospheric absorption of terahertz radiation and water vapor continuum effects. *Journal of Quantitative Spectroscopy and Radiative Transfer*, 127:49–63, 2013. 2
- [31] T. M. Wong, M. Kahl, P. H. Bolívar, and A. Kolb. Computational image enhancement for frequency modulated continuous wave (fmcw) thz image. *J. Infrared, Millimeter, and Terahertz Waves*, 40(7):775–800, 2019. 2, 4
- [32] T. M. Wong, M. Kahl, P. Haring-Bolívar, A. Kolb, and M. Möller. Training auto-encoder-based optimizers for terahertz image reconstruction. In *German Conf. Pattern Recognit.*, pages 93–106, 2019. 2
- [33] B. Yang, L. Ying, and J. Tang. Enhancing bayesian pet image reconstruction using neural networks. In *Proc. IEEE Int. Symp. Biomed. Imag.*, pages 1181–1184, 2017. 4
- [34] H. Chen and Y. Zhang, M. K. Kalra, F. Lin, Y. Chen, P. Liao, J. Zhou, and G. Wang. Low-dose ct with a residual encoder-decoder convolutional neural network. *IEEE Trans. Medical Imag.*, 36(12):2524–2535, 2017. 4
- [35] K. Zhang, W. Zuo and Y. Chen, D. Meng, and L. Zhang. Beyond a Gaussian denoiser: Residual learning of deep

- CNN for image denoising. *IEEE Trans. Image Process.*, 26(7):3142–3155, 2017. 4, 7
- [36] K. Zhang, W.M. Zuo, and L. Zhang. Ffdnet: Toward a fast and flexible solution for cnn-based image denoising. *IEEE Trans. Image Process.*, 27(9):4608–4622, 2018. 4
 - [37] R. Zhang, P. Isola, A.A. Efros, E. Shechtman, and O. Wang. The unreasonable effectiveness of deep features as a perceptual metric. In *Proc. IEEE/CVF Int. Conf. Comput. Vis. Pattern Recognit.*, pages 586–595, 2018. 7
 - [38] Y. Zhang, Y. Tian, Y. Kong, B. Zhong, and Y. Fu. Residual dense network for image restoration. *IEEE Trans. Pattern Anal. Mach. Intell.*, 2020. 4, 7
 - [39] S. Zhou, J. Zhang, J. Pan, H. Xie, W. Zuo, and J. Ren. Spatio-temporal filter adaptive network for video deblurring. In *Proc. IEEE/CVF Int. Conf. Comput. Vis.*, pages 2482–2491, 2019. 4, 5
 - [40] B. Zhu, J. Z. Liu, S. F. Cauley, R. Bruce Rosen, and M. S. Rosen. Image reconstruction by domain-transform manifold learning. *Nature*, 555(7697):487–492, 2018. 4